THE JOURNAL OF PHYSICAL CHEMISTRY C LETTERS

2009, *113,* 31–36
Published on Web 12/10/2008

Discontinuous Growth of Colloidal CdSe Nanocrystals in the Magic Structure

Hsueh Shih Chen* and Ramachandran Vasant Kumar

Department of Materials Science and Metallurgy, University of Cambridge, Pembroke Street, Cambridge CB2 3QZ, U.K.

Received: October 22, 2008; Revised Manuscript Received: November 25, 2008

This study reveals that the growth rate of colloidal CdSe nanocrystals negatively deviates from the prediction of the classic growth theory from thermodynamics as CdSe nanocrystals attain the magic closed-shell structure at around 1.8 nm. We have suggested that the negative deviation is the consequence of the chemical potential well generated from the closed-shell structure of nanocrystals.

1. Introduction

The synthesis of colloidal nanocrystals (NCs) has drawn much attention in science and technology. The initial success of the nonaqueous hot injection approach that employed a combination of trioctylphosphine oxide (TOPO) and trioctylphosphine (TOP) for synthesis of II−VI colloidal NCs has encouraged scientists to develop the fundamentals and industrial applications.[1,2] Subsequent development in NC synthesis such as core/shell structures,[3] size focusing,[4] shape control,[5] and greener synthesis (oxides instead of organometallic precursors)[6] has opened up the possibility of potential applications in numerous areas such as electroluminescent devices,[7] biological indicators,[8] hybrid solar cells,[9] white light emission diodes,[10] and so forth.

Although the hot injection approach has achieved a considerable success in the synthesis of inorganic materials, the growth mechanism has not been completely established yet. For the greener synthesis of CdSe NCs, it has been agreed that injection of a cold precursor (e.g., TOPSe) into a hot Cd precursor with melting surfactants induces a rapid decomposition of precursors and produces monomers at high supersaturation.[11] This event in turn activates homogeneous nucleation. The following temperature drop caused by cold precursors separates the nucleation from the growth process. Therefore, nearly monodispersed NCs can be obtained. Peng and his co-workers have suggested that growth of CdSe NCs in TOPO/hexadecylamine ligands is divided into four stages, that is, particle formation (equivalent to nucleation), size focusing (particle concentration drop and size distribution focused down), stable stage (equilibrium between monomers and NCs), and the stage of defocusing of size (Ostwald ripening).[12] The kinetics and thermodynamics of CdSe NC growth have been also proposed.[13,14] In this paper, we demonstrate that a discontinuous event arises during the CdSe NCs growth. This phenomenon is attributable to the presence of the chemical potential well generated by the closed-shell structure.

2. Experimental Section

2.1. Materials. All chemicals were used as received. Cadmium oxide (purity 99.99%), selenium (purity 99.999%), trioctylphosphine oxide (TOPO) (purity 90%), trioctylphosphine (TOP) (purity 90%), and 1-hexadecylamine (HDA) (purity 90%) were purchased from Aldrich. Stearic acid (SA) (purity 99%) and lauric acid (LA) (purity 99%) were purchased from Lancaster Synthesis. All solvents were purchased from Sigma-Aldrich (analytical grade).

2.2. Synthesis of CdSe NCs. CdSe NCs were synthesized by the standard hot injection approach proposed by Peng et al.[15] HDA was introduced into the process to reduce the size distribution.[16] Briefly, hot CdO precursor was prepared using 0.5 mmol of CdO, 2 mmol of SA or LA, 25 mmol of TOPO, and 40 mmol of HDA at 300 °C in a flask. A cold TOP−Se stock solution was prepared by dissolving 1.5 mmol of Se powder in 2.3 mmol of TOP and 1.2 mL toluene at room temperature. The cold Se solution was rapidly injected into the hot CdO solution, and after the injection, the temperature was controlled at a lower value for NC growth. Typical injection and growth temperatures used were 300 and 280 °C, respectively.

2.3. Optical Property and Estimation of Size. All samples measured by UV−vis optical absorption and photoluminescence were without any purification or size separation to avoid losing small particles. Particle sizes, size distribution, and concentration were translated from the UV first exciton peak energy according to the calibration data in the literature.[17] For temporal evolutions of NC growth, 0.2 mL of aliquots was taken from solution and dispersed in 10 mL of toluene at various time intervals.

3. Results and Discussion

3.1. Temporal Evolution of PL of Spherical CdSe NCs. Products are confirmed as wurtzite CdSe NCs by X-ray analysis (results not shown). The temporal evolution of photoluminescence (PL) and optical absorption spectra of the CdSe NCs are shown in Figure 1. The optical absorption spectra display clear excitonic absorption, as shown in the inset. The first sharp PL peak from the CdSe NCs appears at around 509 nm at three seconds after an injection of the TOPSe. The following PL peaks reveal a typical red shift in wavelength from 509 to 593 nm as time increases from 3 to 420 s, indicating that the CdSe NCs enlarge according to the quantum size effect. After 600 s, the CdSe NCs show no significant change in PL peak position, implying that the growth reaches thermodynamic equilibrium. Non-normalized PL data show that the PL intensity of the CdSe

* To whom correspondence should be addressed. E-mail: hsc28@cam.ac.uk. Tel: +44 1223 334315. Fax: +44 1223 334567.

10.1021/jp809360n CCC: $40.75

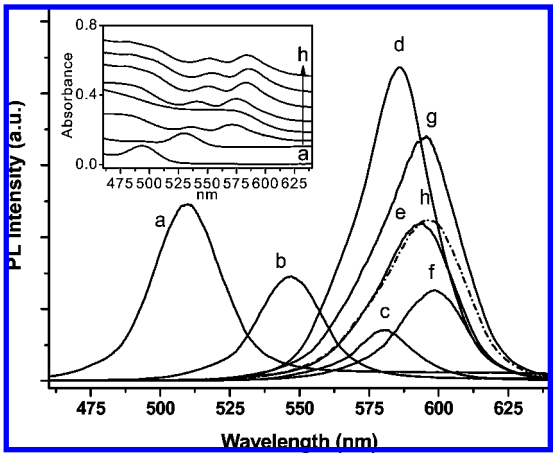

Figure 1. Temporal evolution of PL spectra of NC sampling at 3 (a), 10 (b), 60 (c), 180 (d), 420 (e), 600 (f), 900 (g), and 1200 (h, dashed curve) seconds. The inset displays temporal optical absorption spectra.

NCs is dependent on their size. The PL intensity displays a gradual decrease until a wavelength of 581 nm over a reaction time of 60 s (curves a−c), whereas the maximum intensity dramatically appears at 586 nm at 180 s (curve d). However, the PL intensity decreases again as the peak slightly shifts away from 586 to 592 nm (curve e). In the end, the PL peak locates at 596 nm (curve h). Estimated PL efficiencies of each sample are 0.57 (curve a), 0.49 (curve b), 0.21 (curve c), 0.48 (curve e), 0.26 (curve f), 0.73 (curve g), and 0.55 (curve h) relative to that of 586 nm, appearing in curve d as a relative maximum.

3.2. CdSe NCs in the Closed-Shell Structure. The maximum PL intensity at a wavelength of 586 nm, corresponding to a radius of about 1.8 nm, is attributable to the consequence of the closed-shell structure for CdSe NCs.[18,19] It has been known that the surface structure significantly affects the NC density of states that dominates the optical properties of NCs. For example, surface dangling bonds of NCs may produce nonradiative defects that reduce the luminescence efficiency of NCs.[20,21] Moreover, computer-aided simulation indicates that magic-size CdSe clusters show a well-defined optic gap.[18] Conversely, surface atoms with missing bonds of nonmagic-size CdSe clusters cause relatively small non-well-defined gaps, leading to a reduction in the optic gap. The result of the magic clusters has been extended to explain that CdSe NCs that are 1.1 or 1.7 nm in radius display relatively high PL efficiency as the CdSe NCs have the closed-shell structure and contain the least dangling bonds. This point of view has been verified by chemical etching experiments of CdSe NCs.[19] TEM images in the present study also support this viewpoint, as shown in Figure 2. A portion of CdSe NCs presenting projections perpendicular to the (001) and (100) directions show a closed-shell-like morphology. Note that the edges of some CdSe NCs might lose contrast due to a deficient signal from interference of the electron beam. Theoretically, molecular clusters tend to thermodynamically maximize their bonding and form stable crystallographic configurations.[22] Accordingly, the appearance of the closed-shell morphology in the present study is reasonable as morphologies like ball-like closed-shell structures having lower surface energy are favored in the thermodynamic regime for NCs. Indeed, in the present study, CdSe NCs reach equilibrium at PL wavelengths around 598 nm (radius $\sim$ 2 nm), as shown in curves f−h in Figure 1; therefore, the 1.8 nm CdSe NCs are already in a low supersaturation. The relative low PL intensity for NCs in non-closed-shell morphology, for example, as in curves b and c, is attributed to the presence of additional nonradiative dangling bonds. Moreover, the fluctuation of the PL intensity in the equilibrium state shown in curves f−h is considered to be the cause of the fluctuation of the monomer concentration that would result in a change in the surface morphology of the NCs.

3.3. Discontinuous Growth at the Magic Closed-Shell. Figure 3 shows the PL intensity and crystal radius of CdSe NCs grown in both stearic acid (SA) and lauric acid (LA) as a function of growth time. Both SA and LA data suggest that CdSe NCs have the highest PL efficiency as their radii reach about 1.8 nm at 180 s. The increases in radius of the CdSe NCs in both fatty acids start with an exponential growth in the initial stage until the radius rises to around 1.7 nm, and then, the rate of growth obviously slows down and turns into a linear-like curve, as shown in curves LA and SA in Figure 3. Bullen et al. reported that the increase in the crystal radius as a function of growth time is compatible with the exponential function based on the classic growth theory for CdSe in octadecene.[14] Fitting an exponential curve to our experimental data, interestingly, both SA and LA data show a similar deviation from about 1.7 nm. Carefully examining the data from Bullen et al., a similar tendency at around 1.7 nm can be discerned, although the deviation is small and within the error range.[14] Because the closed-shell size of CdSe NCs just locates on the deviation range of the radius−time curve, it is logical to assume that the closed-shell structure correlates the deviation of the growth curve.

Figure 4 presents the growth rate on the logarithmic scale in relation to the radius for the CdSe NCs. Note that the curve of the growth rate of the CdSe NCs grown in SA and LA deflects from linearity to a much lower value in the range of 1.7−1.8 nm, which is exactly around the size of the closed-shell structure mentioned above. A curve estimated by the experimental results from Bullen et al. also exhibits a similar trend, although the decrease of the growth rate is not as much as that of SA or LA in the present study, which might be the differences in the nature of the surfactants and the experimental conditions between both studies. These results suggest that at least two different growth modes are present in the NC growth instead of a simply continuous process. In the first phase, from the beginning to 1.7 nm, the tendency of exponential decay in the growth rate in the initial stage is consistent with the prediction made by the classic growth theory. In the second phase, the negative deviation starting from around 1.7 nm is thought to be the consequence of the closed-shell morphology for the CdSe NCs.

3.4. Chemical Potential Well in NC Growth. Like inert gases with atomic shells filled by electrons based on the Pauli Exclusion Principle, which have the maximum ionization potential as a function of atomic number, the electric magic number can arise for atomic clusters, and the structural magic number can arise for NCs. This will correspond to some unique sizes, for example, the closed-shell size for NCs without reactive atoms or clusters on the surface, and thus, all reactive chemical energy levels are filled. With the closed-shell morphology, which means that the NC surface is stacked by the most coordinated atoms, NCs are thermodynamically more stable than any other size deviating slightly. In other words, the closed-shell NCs may be thought to be in a stable or quasi-stable state. We assumed that the state would result in a deviation to some extent of the classic size−chemical potential curve from the thermodynamics for crystal growth.

In order to examine the energy potential well, we conducted kinetic perturbation and thermal annealing experiments for the closed-shell CdSe NCs. In the kinetic perturbation experiment,

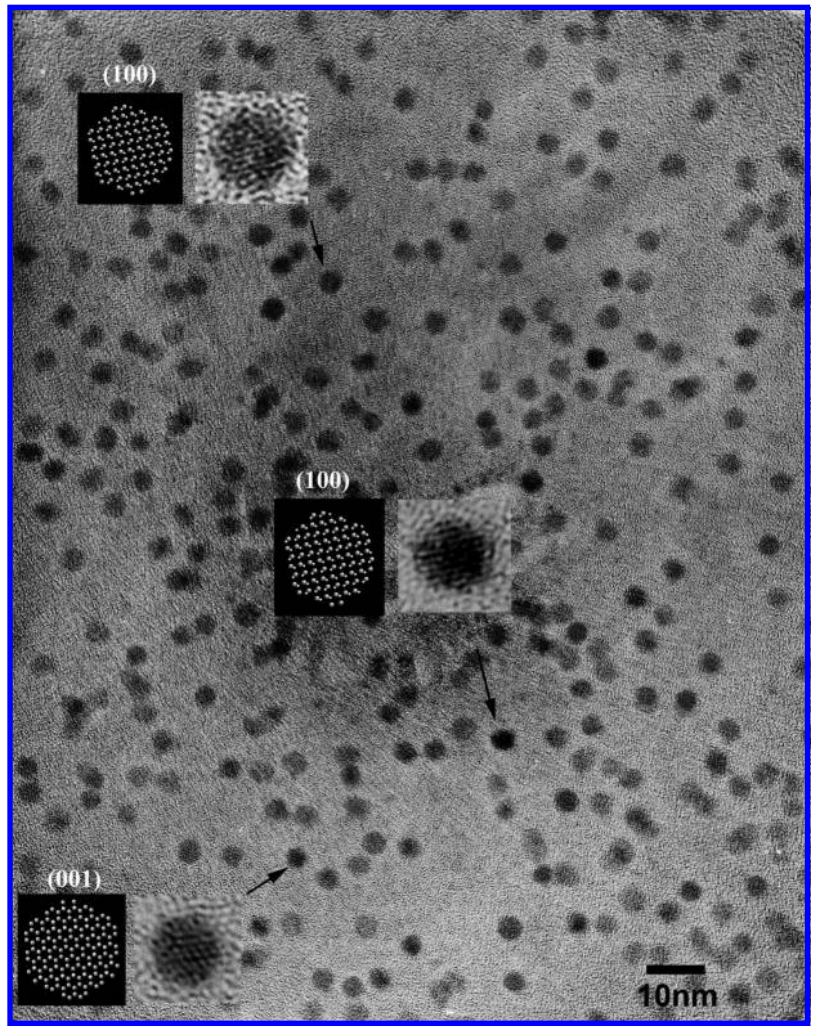

Figure 2. TEM image of CdSe NCs taken in the bright field and simulated atomic images (1.75 nm).

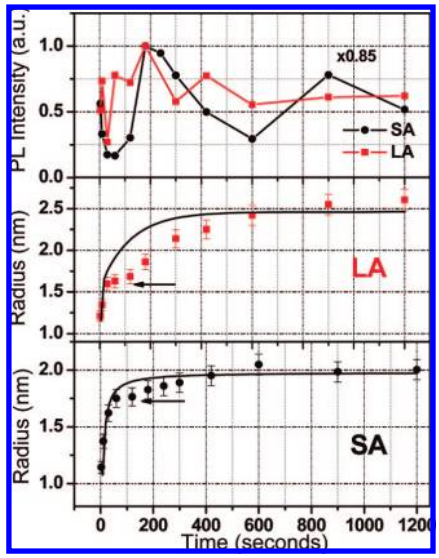

Figure 3. Variations in PL intensity and radius with reaction time for CdSe NCs synthesized with two different fatty acids, stearic acid (SA) and lauric acid (LA).

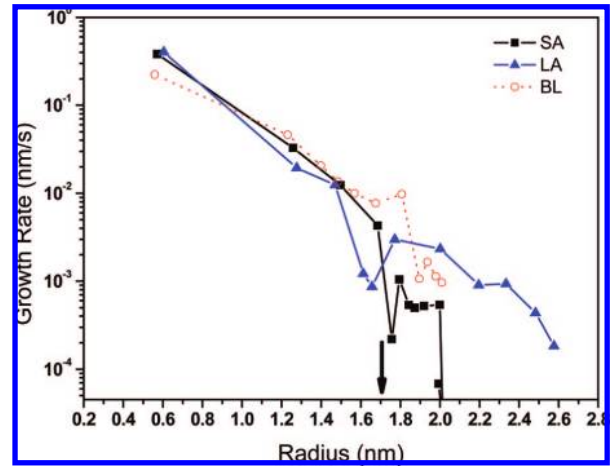

Figure 4. The growth rates of the NCs synthesized in SA and LA on the logarithmic scale as a function of radius. The red dashed curve BL was estimated and plotted according to the experimental data of NC grown in noncoordinating octadecene from Bullen et al.[14] The growth rates are estimated at middle points between two measured sizes.

we suspended the growth of CdSe NCs by quenching the reaction system temperature from 280 to 120 °C as the CdSe NCs attained a closed-shell size. Then, five extra injections of TOPSe were successively injected into the reaction system every minute (each injection contains 0.285 mmol of Se). As shown in Figure 5a, the removal of thermal energy does not change the PL peak position, indicating that the crystal growth is effectively suspended. Moreover, the five extra injections of TOPSe show no effect on the PL peak position for the closed-shell CdSe NCs as well. In general, any temperature or concentration variation should alter the crystal size according

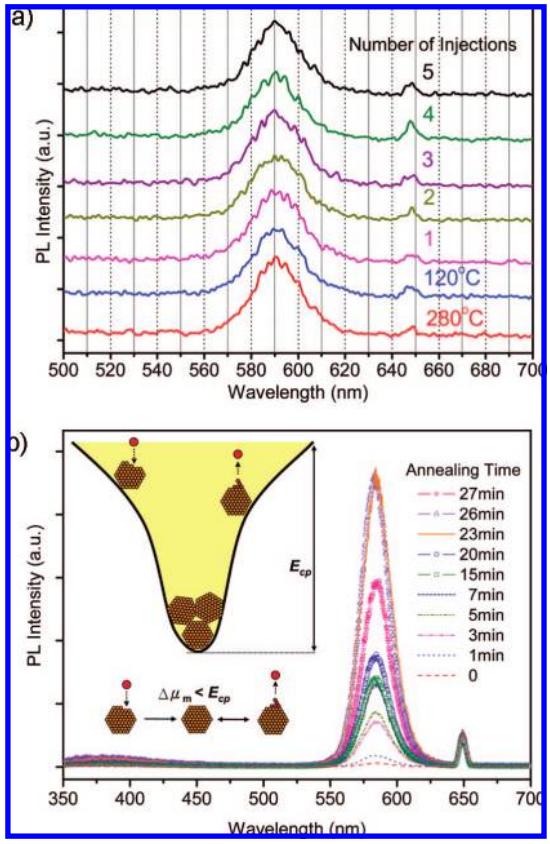

Figure 5. (a) Kinetic perturbation experiment at 120 °C. Extra injections were carried out every minute for five times. (b) Thermal treatment of the closed-shell CdSe NCs at 150 °C. The inset shows that the closed-shell NCs are constrained in the chemical potential well.

to the Gibbs−Thomson relationship. Thus, this event demonstrates that the closed-shell CdSe NCs indeed stay in a certain stable state, where they are constrained by a certain potential energy that is higher than the overall chemical potential of monomers from the system and the extra injections. On the other hand, in a thermodynamic regime, crystals should automatically "centralize" into the stable state to minimize the free energy. Figure 5b shows PL spectra from the closed-shell CdSe NCs annealed at 150 °C. Enhancement of the PL intensity implies that the number of the closed-shell CdSe NCs increases with annealing time. Also, the standard deviation of the NC size gradually decreases from 0.22 to 0.19 nm, indicating that more and more NCs centralize into the closed-shell size. These results prove that the closed-shell structure generates a stable state so that those NCs slightly deviating from the size would tend to gain the closed-shell morphology. This relatively stable state can appear in the classic size−chemical potential growth curve for crystal growth. Therefore, we define this relative stable state as the chemical potential well. The inset in Figure 5b illustrates the chemical potential well with the potential energy $\boldsymbol{E}_{\mathbf{cp}}$. The drop in the PL intensity at 27 min is attributed to the decrease in the number of the closed-shell CdSe NCs caused by temperature fluctuation from the heating source.

The emergence of the chemical potential well infers that NCs will somewhat refuse additional monomers to integrate into their surface lattices if no sufficient chemical energy is supplied from system. Practically, this event may reveal a growth bottleneck and depress crystal growth. Accordingly, the negative deviation in the second phase mentioned above is caused by the chemical potential well, as shown in Figure 4. The growth bottleneck has also been found in the previous study.[1]

3.5. Surface Nucleation in NC Growth. Normally, the crystal growth rate should slow down and become zero at the end of a reaction. However, it is interesting that the slopes of all curves in Figure 4 evolve from being negative to positive, indicating that the growth rate of the CdSe NCs inversely increases. At constant temperature and pressure, the crystal growth rate in solution is determined by the difference in free energy or chemical potential ($\mu_i = \partial G/\partial N_i$) between the crystal surface and monomers. In the initial stage, an injection of Se precursors into Cd precursors provides sufficient chemical potential for the nucleation and the subsequent growth process. The decreasing supersaturation of monomers eventually causes the growth rate to slow as the overall chemical potential decreases.[14] If the $\Delta\mu$ becomes zero, the growth stops, and the reaction reaches equilibrium. The growth rate of crystals can be derived from the net rate of consumption of monomers, which is related to the net rate of adsorption−desorption of monomers on the surface of NCs or the hopping frequency, considering the interfacial barrier of the monomers from solution to the crystal surface. Therefore, the crystal growth is assigned to a number of successful hops of monomers to the crystal surface after overcoming the activation energy. The number of energetic monomers (N_i^*) at the energy state i obeys the Boltzmann distribution, that is, $N_i^* \propto \exp(-G_i/kT)$. The growth rate is related to the thermal energy and proportional to the N_i^*. Therefore, it could be expressed as in the form of the Arrhenius equation

$$\frac{\mathrm{d}r}{\mathrm{d}t} \propto \exp\left(\frac{-\Delta G_{r-r'}}{kT}\right) \tag{1}$$

where $\mathrm{d}r/\mathrm{d}t$ is the growth rate of crystals, k is the Boltzmann constant, and T is temperature. $\Delta G_{r-r'}$ is the free-energy difference between r and r' for spherical particles and is determined by the summation of the volume free-energy change $[(4/3)\pi r^3 \Delta g_v]$ and the surface energy change $(4\pi r^2\sigma)$ and the interface energy barrier. If the interface energy barrier is ignored, the $\Delta G_{r-r'}$ is associated with the concentration of monomers in solution, according to the Gibbs−Thomson relationship, which gives the size-dependent supersaturation for NCs

$$\ln(C_{\mathrm{NC}}/C_{\mathrm{Bulk}}) = \frac{2\sigma V_{\mathrm{m}}}{rkT} \tag{2}$$

The ratio of $C_{\mathrm{NC}}/C_{\mathrm{Bulk}}$ is defined as supersaturation (S), σ is the surface energy, V_{m} is the molecular volume, and r is radius of NCs. C_{NC} and C_{Bulk} are values of the solubility for NCs and the bulk, respectively. In equilibrium, the solubility of NCs is exactly the same as the concentration of monomers. Therefore, the net growth rate slows down with time as supersaturation S reduces. However, Figure 4 clearly shows that the CdSe NC growth rate rises as their radius just passes the closed-shell size. It is unlikely that the chemical potential suddenly elevates from a fluctuation of the concentration or from a change in the composition of the solution since the reaction temperature is held constant and no extra injections are introduced. As the system is still away from the final equilibrium state, it could be suggested that a specific process emerges.

As mentioned above, the closed-shell NCs are in a relatively stable state and somewhat refuse additional monomers to integrate into their surface lattices. If energetic monomers surpass the chemical potential well barrier $\boldsymbol{E}_{\mathbf{cp}}$ and form stable clusters on the closed-shell NCs, the crystal growth could carry on. This process may be considered a surface nucleation process on the NCs. The surface nucleation is a two-dimensional (2D) growth, in which the total free energy is scaled with surface

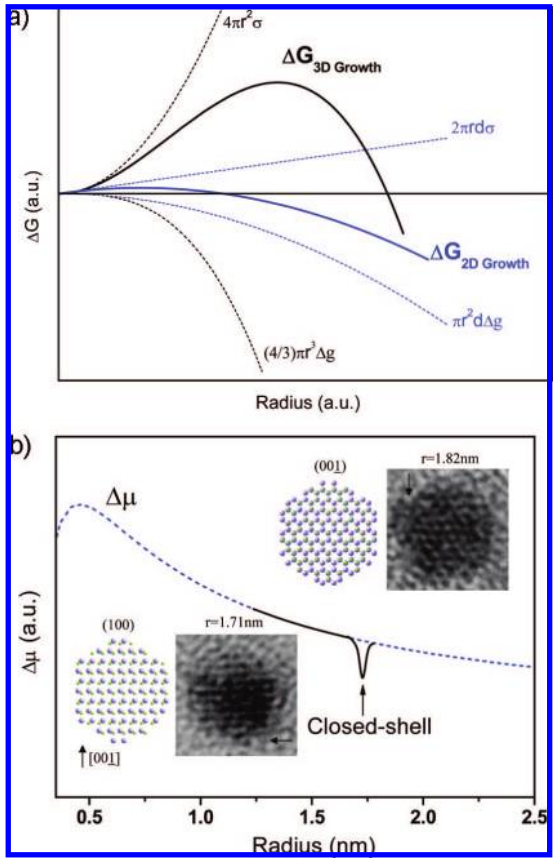

Figure 6. (a) Free energy−radius diagram for 2D and 3D nucleation, where r, σ, Δg, and d are the NC radius, surface energy, volume free energy, and atomic diameter, respectively. (b) Simulated curve of NC growth that indicates the chemical potential well caused by the closed-shell morphology. The insets show CdSe TEM images at around the closed-shell size together with simulated atomic images of CdSe NCs at 1.75 nm.

area ($\propto r^2$) rather than volume in a three-dimensional (3D) growth. Similarly, the increase of the surface energy of a 2D cluster ($\propto r$) is slower than that of a free-standing particle when the particle size increases. Accordingly, both the critical size and critical energy of 2D nuclei are smaller than those of free-standing 3D nuclei for materials in the same composition, as shown in Figure 6a. Note that a change in the slope of the free energy for 2D growth is smaller than that of 3D growth as $r > r^*$, stating that the driving force needed for 2D growth is much smaller. This indicates that the surface nucleation is able to take place in a low supersaturation. Consequently, the surface nucleation would occur in the growth process as the closed-shell NCs grow over the closed-shell size. Figure 6b presents a chemical potential−radius curve including the chemical potential well at the closed-shell size. The insets in Figure 6b display TEM images of the CdSe NCs around the closed-shell size together with simulated atomic images of CdSe NCs. The images show that atomic clustering takes place on the NC surface.

Introduction of the chemical potential well together with the surface nucleation brings some insight into growth fundamentals for NCs. For example, NC growth may happen at those high-energy sites where surface nuclei can nucleate with lower energy such as (00$\underline{1}$) and (111) for wurtzite and zinc blende NCs, respectively.[23,24] Thus, hexagonal wurtzite crystals tend to grow along the c-axis and form nonspherical particles. In this case, the dimension of the facet (00$\underline{1}$) might be an important factor as adsorbed monomers may not form a stable nucleus until it exceeds the critical size.

The size corresponding to the maximum PL intensity measured in the present study is slightly different from that in the previous etching study, in which the maximum PL efficiency of CdSe NCs was shown to be 580 nm, corresponding to 1.7 nm in radius.[18] It is seen that the mean size of CdSe NCs in the chemical potential well in the growth study would be slightly larger than that from the etching experiment. This is due to the $\Delta\mu$ for crystal growth, which not only prevents the closed-shell NCs from dissolution to a non-closed-shell structure but is a benefit for the adsorption of monomers on the closed-shell NCs to diminish the energy difference between monomers and the NCs before the surface nuclei form. Therefore, the measured size of CdSe NCs in the growth experiment would be slightly larger than that in an etching experiment that has an inverse situation.

For the CdSe NCs, 1.1 nm is also reported as closed-shell size.[25,26] In the present study, although it is difficult to collect enough data before 3 s of reaction time, CdSe NCs at around 1.1 nm were always produced at around 3 s after the injection of precursors. This may be due to the fact that the CdSe NCs are relatively stable and have a slower growth rate. Moreover, it is believed that there are other types of the chemical potential wells, which are formed either by the closed-shell structures or other magic-structured morphologies such as the core−cage CdSe NCs.[22]

4. Conclusion

We have conducted temporal evolution of photoluminescence and transmission electron microscopy analyses to show that CdSe NCs at around 1.8 nm have the magic closed-shell structure. In the growth experiment, a negative deviation in the growth rate, which does not obey the classic growth kinetics from thermodynamics, is found to take place as CdSe NCs reach the closed-shell size. We have suggested that the negative deviation is the consequence of the chemical potential well generated from the closed-shell structure for CdSe NCs. These results are expected to lead to further development in the field of nucleation and growth for nanoscale materials.

References and Notes

(1) Murray, C. B.; Norris, D. J.; Bawendi, M. G. *J. Am. Chem. Soc.* **1993**, *115*, 8706–8715.
(2) Puntes, V. F.; Krishnan, K. M.; Alivisatos, A. P. *Science* **2001**, *291*, 2115–2117.
(3) Hines, M. A.; Guyot-Sionnest, P. *J. Phys. Chem.* **1996**, *100*, 468–471.
(4) Peng, X.; Wickham, J.; Alivisatos, A. P. *J. Am. Chem. Soc.* **1998**, *120*, 5343–5344.
(5) Peng, X.; Manna, L.; Yang, W.; Wickham, J.; Scher, E.; Kadavanich, A.; Alivisatos, A. P. *Nature* **2000**, *404*, 59–61.
(6) Peng, Z. A.; Peng, X. *J. Am. Chem. Soc.* **2001**, *123*, 183–184.
(7) Colvin, V. L.; Schlamp, M. C.; Alivisatos, A. P. *Nature* **1994**, *370*, 354–357.
(8) Bruchez, M., Jr.; Moronne, M.; Gin, P.; Weiss, S.; Alivisatos, A. P. *Science* **1998**, *281*, 2013–2016.
(9) Huynh, W. U.; Dittmer, J. J.; Alivisatos, A. P. *Science* **2002**, *295*, 2425–2427.
(10) Chen, H. S.; Hsu, C. K.; Hong, H. Y. *IEEE Photonics Technol. Lett.* **2006**, *18*, 193–195.
(11) Talapin, D. V.; Rogach, A. L.; Haase, M.; Weller, H. *J. Phys. Chem. B* **2001**, *105*, 12278–12285.
(12) Qu, L.; Yu, W. W.; Peng, X. *Nano. Lett.* **2004**, *4*, 465–469.
(13) Peng, Z. A.; Peng, X. *J. Am. Chem. Soc.* **2002**, *124*, 3343–3353.
(14) Bullen, C. R.; Mulvaney, P. *Nano. Lett.* **2004**, *4*, 2303–2307.
(15) Qu, L.; Peng, Z. A.; Peng, X. *Nano. Lett.* **2001**, *1*, 333–337.
(16) Reiss, P.; Bleuse, J.; Pron, A. *Nano. Lett.* **2002**, *2*, 781–784.

(17) Yu, W. W.; Qu, L.; Guo, W.; Peng, X. *Chem. Mater.* **2003**, *15*, 2854–2560.
(18) Yu, M.; Fernando, G. W.; Li, R.; Papadimitrakopoulos, F.; Shi, N.; Ramprasad, R. *Appl. Phys. Lett.* **2006**, *88*, 231910.
(19) Yu, M.; Fernando, G. W.; Li, R.; Papadimitrakopoulos, F.; Shi, N.; Ramprasad, R. *J. Comput.-Aided Mater Des.* **2007**, *14*, 167–174.
(20) Rodriguez-Viejo, J.; Jensen, K. F.; Mattoussi, F.; Michel, J.; Dabbousi, B. O.; Bawendi, M. G. *Appl. Phys. Lett.* **1997**, *70*, 2132.
(21) Chen, H. S.; Lo, B.; Hwang, J. Y.; Chang, G. Y.; Chen, C. M.; Tasi, S. J.; Wang, S. J. *J. Phys. Chem. B* **2004**, *108*, 17119–17123.
(22) Kasuya, A.; Sivamohan, R.; Barnakov, Y. A.; Dmitruk, I. M.; Nirasawa, T.; Romanyuk, V. R.; Kumar, V.; Mamykin, S. V.; Tohji, K.; Jeyadevan, B.; Shinoda, K.; Kudo, T.; Terasaki, O.; Liu, Z.; Belosludov, R. V.; Sundararajan, V.; Kawazoe, Y. *Nat. Mater.* **2004**, *3*, 99–102.
(23) Pneg, X. *Adv. Mater.* **2003**, *15*, 459–469.
(24) Manna, L.; Scher, E. C.; Alivisatos, A. P. *J. Cluster Sci.* **2002**, *13*, 521–532.
(25) Soloviev, V. N.; Eichhofer, A.; Fenske, D.; Banin, U. *J. Am. Chem. Soc.* **2000**, *122*, 2673–2674.
(26) Kudera, S.; Zanella, M.; Giannini, C.; Rizzo, A.; Li, Y.; Gigli, G.; Cingolani, R.; Ciccarella, G; Spahl, W.; Parak, W. J.; Manna, L. *Adv. Mater.* **2007**, *19*, 548–552.

JP809360N